

## Antimicrobial and Anticorrosive Activity of Adsorbents Based on Chitosan Schiff's Base

Riham R. Mohamed\*, A.M. Fekry

Faculty of Science- Cairo University - Department of Chemistry - Giza 12613, Egypt

\*E-mail: [rihamrashad@hotmail.com](mailto:rihamrashad@hotmail.com)

Received: 17 March 2011 / Accepted: 30 May 2011 / Published: 1 July 2011

---

Characterization and synthesis for a novel schiff's base of chitosan was investigated. Swell ability of schiff's base of chitosan in different buffered solutions was shown to be higher than that of native chitosan in neutral and basic pH values. The antimicrobial activities of both chitosan and its schiff's base towards *E. coli*, *S. aureus*, *A. niger* and *Candida albicans* were investigated and found to be stronger for chitosan schiff's base. Chitosan-Crotonaldehyde Schiff's Base (Ch-Cr-SB) coated AZ91E alloy has been synthesized chemically and its metal and dye uptake were investigated in comparison with parent chitosan. The electrochemical corrosion behavior has been also studied for Ch-Cr-SB in aerated 3% NaCl solution containing different concentrations of schiff's base, in the range from 0.03 to 0.075 mM, using different techniques. Results showed that corrosion rate decreases with increasing the polymer concentration or immersion time, however, it increases with increasing temperature from 298 to 328 K.

---

**Keywords:** Chitosan Schiff's base, antimicrobial activity, crotonaldehyde, Swellability, Corrosion.

### 1. INTRODUCTION

Chitosan, as a natural renewable resource, possesses unique properties such as biocompatibility, biodegradability, non-toxicity and has important applications in the biomedical, agriculture, wastewater purification, environmental protection, biotechnology, and cosmetics domains. Chitosan has both reactive amino and hydroxyl groups that can be used to chemically alter its properties under mild reaction conditions.

Among these substituted biopolymers there are the schiff's bases, obtained by the reactions of the free amino groups of chitosan with an active carbonyl compound such as aldehyde or ketone [1-4]. These bases present the characteristic imine group ( $-RC=N-$ ) in their structures [5] and offer several possibilities such as in reactions requiring the protection of chitosan C<sub>2</sub> amino groups [6-7] or in

reactions with metal ions for enhancing the complexation properties of the biopolymer yielding a material with potential analytical and environmental applications [8-13]. Some papers concerning the thermal behavior study of some biopolymeric schiff's bases prepared from chitosan have been reported [14-15]. Chitosan has widely been studied for pollutants adsorption from aqueous solutions.

Chitosan cationic character, along with the presence of reactive functional groups in its polymeric chains, has given it particular possibilities as an efficient adsorbent. It is evident from literature data that this biopolymer offers a great potential in the adsorption field for environmental purposes [16-18].

In particular, one of the major applications for chitosan is based on its ability to bind strongly heavy and toxic metals [16]. Recently, numerous studies on chitosan-based biomaterials for dye removal showed that these biosorbents are very efficient and have a high affinity for many classes of dyes [19-22].

In the present study, chitosan-crotonaldehyde schiff's base was prepared through introducing more good chelating groups like (-N=CH-) into the chitosan polymeric chains. Ch-Cr-SB was investigated as good adsorbent for different metal ions like; Ni<sup>2+</sup>, Co<sup>2+</sup>, Cd<sup>2+</sup> and Cu<sup>2+</sup> and also as good adsorbent for different types of dyes like; Maxilon blue (*Cationic dye*) and Congo red dye (*Acidic dye*). It has been shown that schiff's base chitosan derivative is having strong antibacterial and antifungal activity. Also, it has been evaluated as an eco-friendly corrosion inhibitor for metal alloys as AZ91E alloy.

Magnesium alloys [23-26] are the lightest of all the structural metals with good strength/weight ratio and castability. The AZ91 (nominally 9 wt.% Al and 1 wt.% Zn) series of alloys constitute approximately 85% of all Mg-based alloys used in industry as they provide a good compromise of mechanical properties, castability and an industrially accepted appropriate base level corrosion resistance for numerous applications.

AZ91E is a widely used magnesium-based alloy, which exhibits a balance between mechanical properties and moderate corrosion resistance. Many researches concerning the synthesis, characterization and thermal behavior of some biopolymeric schiff's bases prepared from chitosan have already been reported [12-14] but no literature was reported about its corrosion behavior on AZ91E alloy.

Thus, in this study, synthesis and characterization of Chitosan-Crotonaldehyde Schiff's Base (Ch-Cr-SB) via several analyses like ; IR, XRD ,SEM and thermal analyses were done.

Swellability properties were investigated in different buffered solutions, metal and dye uptake were studied and also the antimicrobial activity of the schiff's base was investigated against *Escherichia coli*, *Staphylococcus aureus*, *Aspergillus niger* and *Candida albicans*.

Also, this work explores the effect of a (Ch-Cr-SB) coating polymer of high antimicrobial activity on the corrosion behavior of AZ91E alloy in naturally aerated artificial sea water (3% NaCl).

The high antibacterial activity means that the formed polymer coated film is not affected by the fungi or bacteria adhered in the medium around the metal alloy. Corrosion behavior is studied using potentiodynamic polarization, electrochemical impedance spectroscopy (EIS) measurements and surface examination via scanning electron microscope (SEM) technique.

## 2. EXPERIMENTAL SECTION

### 2.1. Materials

Chitosan (code KB-002) was purchased from Funakoshi Co. LTD, Japan. (Deacetylation content = 89 %), Crotonaldehyde was obtained from (Sigma). *Congo red dye* (Acidic dye) and *Maxilon Blue dye* (cationic dye) was purchased from G.T.Gurr, London, s.w.6. All other reagents were of analytical grade, used without further purification.

### 2.2. Instrumentals

FTIR spectra were recorded in KBr discs on (FTIR model 8000) Testcan Shimadzu IR-Spectrometer under dry air at room temperature within the wave number range of 4000-600  $\text{cm}^{-1}$ .

Thermogravimetric analysis was done on TGA-50H Shimadzu thermogravimetric analyzer. Samples were heated from 0 to 500 °C in a platinum pan with a heating rate 10 °C / min, in  $\text{N}_2$  atmosphere of flow rate 25 mL / min.

X ray Diffraction was done using Bruker D<sub>8</sub> Advance, at 40 KV, 40 mA using target Cu K $\alpha$  with secondary monochromator- Germany.

The dry sample, spread on a double sided conducting adhesive tape, pasted on a metallic stub, was coated with a gold layer of 100  $\mu\text{m}$  thickness using an ion sputter coating unit (JEOL S150A) for 2 min and observed in a JEOL-JXA-840A Electron probe microanalyzer at 20 KV.

Atomic absorption was done on AAnalyst 100 winlab-Perkin Elmer to determine the amount of metal ions remaining in the polymer liquor.

Colorimetric Spectrophotometric analyses were done on Unico 1200 Spectrophotometer at  $\lambda_{\text{max}}$  480 nm for Congo red dye and  $\lambda_{\text{max}}$  580 nm for Maxilon blue dye.

### 2.3. Electrochemical Instrumentation

The cell used was a typical three-electrode one fitted with a large platinum sheet of size 15 x 20 x 2 mm as a counter electrode (CE), saturated calomel (SCE) as a reference electrode (RE) and the alloy as a working electrode (WE).

The impedance diagrams were recorded at the free immersion potential (OCP) by applying a 10 mV sinusoidal potential through a frequency domain from 10 kHz down to 100 mHz. Cathodic and anodic polarization curves were scanned from -1.8 V to -0.8 V with a scan rate of 1  $\text{mV s}^{-1}$ . The electrochemical experiments were always carried inside an air thermostat which was kept at 25 °C, unless otherwise stated.

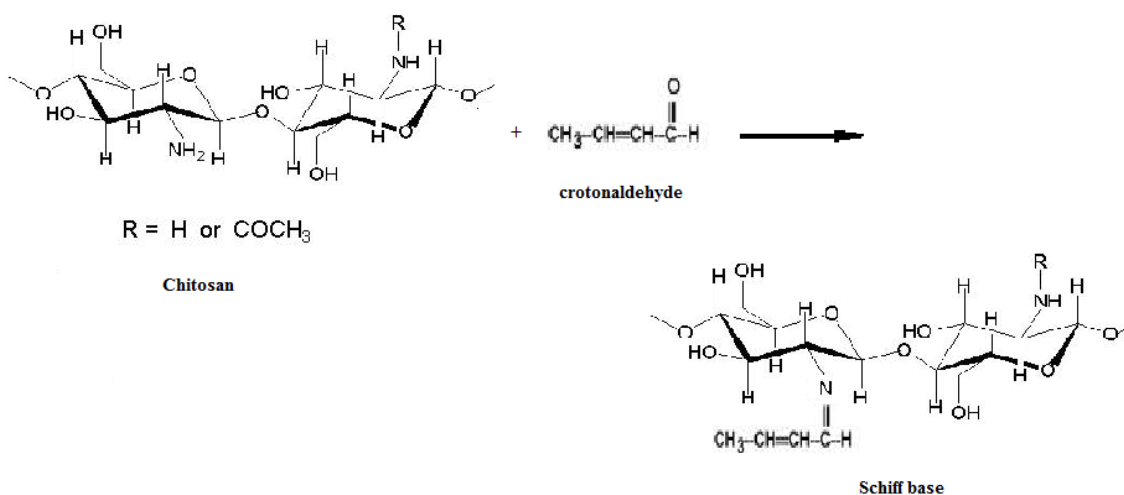
All potentials were measured and given with respect to SCE ( $E = 0.241 \text{ V/SHE}$ ). The instrument used is the electrochemical workstation IM6e Zahner-elektrok, GmbH, (Kronach, Germany).

## 2.4. Antimicrobial assays

Antimicrobial activity of the investigated samples was determined using a modified disc diffusion method

## 2.5. Preparation of Schiff's base polymer (Ch-Cr-SB)

Schiff's base was synthesized according to the procedure reported in literature [27] by dissolving 400 mg of the chitosan with 25 mL of 0.15 M acetic acid solution in a thermostated reactor at 25 °C for 12 h, till complete formation of the polymer in hydrogel form. Then, a predetermined amount of crotonaldehyde dissolved in 10 mL ethanol was added to the chitosan solution. Deep yellow gels of schiff's base were formed and collected by filtration, washed several times with ethanol to remove any unreacted materials, dried at 60 °C under reduced pressure giving a yellow powder.



**Scheme 1.** Schematic diagram of schiff base Chitosan - crotonaldehyde (Ch-Cr-SB) formation

## 2.6. Water uptake

Water uptake of Chitosan and Ch-Cr-SB were studied at 30 °C in different buffered solutions of different pH values; 4, 7 and 9. A known amount of pre-dried sample was placed into a flask with 25 mL buffer solution of a given pH and kept undisturbed in a thermo-stated bath (at 30 °C) until equilibrium swelling was attained after 24 hours. The swollen sample was taken off and the surface was quickly wiped off by absorbent paper just to remove the droplets on the surface and then reweighed. The results obtained represent the average of three comparable experiments for each sample.

$$\text{Water uptake percentage} = (W_s - W_o) / W_o \times 100$$

$W_s$  = weight of wet sample.

$W_o$  = weight of dry sample.

### 2.7. Metal ion uptake

A definite weight of either chitosan or Ch-Cr-SB was soaked in the chloride salts solutions of known concentrations for various heavy metal ions like:  $\text{Ni}^{2+}$ ,  $\text{Co}^{2+}$ ,  $\text{Cd}^{2+}$  and  $\text{Cu}^{2+}$  and kept till equilibrium (for 24 hours). The strength of unabsorbed metal salt solutions was determined by atomic absorption technique. This experiment was done in triplicate.

### 2.8. Dye uptake

Two examples for dyes were used; Congo red (*acidic dye*) and Maxilon Blue (*cationic dye*). 25 mL of the dye solution of a known concentration was added to 100 mg of chitosan and Ch-Cr-SB, respectively, in 100 mL flat bottomed flask with a ground joint stopper and stirred continuously at room temperature for 24 hr to reach equilibrium. After filtration, the concentration of the dye in the filtrate was determined colourimetrically at wavelength 480 and 580 nm, for Congo red and Maxilon Blue dyes, respectively.

This experiment was done in triplicate. The quantity of adsorbed dye (Q) was calculated according to the following equation:

$$Q = (N_a - N_s)/W$$

Where:

Q = fixed quantity of dye (mg) / weight of the substrate (g).

$N_a$  = Quantity of original dye (mg).

$N_s$  = Quantity of remaining dye in the solution after adsorption (mg).

W = mass of the substrate (g)

### 2.9. Preparation of electrode

An extruded magnesium aluminum alloy (AZ91E) -donated from Department of mining, Metallurgy and Materials Engineering, Laval University, Canada- with composition (wt%): 9.0 Al, 0.7 Zn, 0.13 Mn, 0.03 Cu, 0.01 Si, 0.006 Fe, 0.004 Ni, 0.0007 Be and balance Mg were tested in the present study. The coupon was welded to an electrical wire and fixed with Araldite epoxy resin in a glass tube leaving cross-sectional area of the specimen  $0.196 \text{ cm}^2$ .

The surface of the tested electrode was mechanically polished by emery papers with 400 up to 1000 grit to ensure surface roughness. The substrates were dipped for 3 hours into various concentrations of Ch-Cr-SB solution (dissolved in 1% acetic acid solution) and then pulled up and this process was repeated 6 times. The coating films thus obtained were dried at  $80 \text{ }^\circ\text{C}$  for 2 h before characterization.

## 2.10. Microorganisms and in vitro antimicrobial assays

### 2.10.1. Antibacterial assay

Antimicrobial activity of the investigated samples was determined using a modified disc diffusion method. *E. coli* and *S. aureus* were used as the investigated organisms. A representative microbe colony was picked off, placed in nutrient broth then incubated in an air-bath shaker at 37 °C for 24 h. By appropriately diluting with sterile normal saline (0.9%) solution, the cultures of *E. coli* and *S. aureus* containing ~10<sup>7</sup> CFU/mL were prepared and used for the antibacterial test. The antibacterial effect of chitosan and its schiff's base against *E. coli* and *S. aureus* were measured optically at 620 nm. The bacterial suspension, 0.2 mL was inoculated under aseptic conditions into 100 mL liquid peptone medium (1 % peptone, 0.3 % beef extract and 0.5 % NaCl) containing chitosan or its schiff's base that had been sterilized at 121 °C for 20 min. Standard disc of *Tetracycline* (antibacterial agent), and *Amphotericin B* (Antifungal agent) served as positive controls for antimicrobial activity but filter discs impregnated with 10 µl of solvent (distilled water, chloroform, DMSO) were used as a negative control. All the samples were incubated at 37 °C with shaking.

The inhibition effect of chitosan and its schiff's base on growth of *E. coli* and *S. aureus* were investigated using agar plates. The peptone culture plates were prepared, in which 0.1 mL solution of bacterial suspension was first added then 0.1 mL solution of chitosan with different concentrations. Both of them were spread uniformly. A blank without chitosan was prepared for comparison. All the plates were incubated at 37 °C for 24 h. Then the plates were taken out of the incubator and the inhibition rate was calculated. The inhibition rate was defined as:

$$\eta = (N_1 - N_2) / N_2$$

Where  $N_1$  and  $N_2$  are the number of colonies on the plates before and after inhibition, respectively. The area of no organism growth around the disc is known as a “**Zone of inhibition**” or “**Clear zone**”.

### 2.10.2. Antifungal assay

*A. niger* and *Candida albicans* were used as the test organisms. A representative microbe colony was picked off with a wire loop, placed in liquid Sabouraud medium and then incubated in an air-bath shaker at 28 °C for 7 days. The inhibition of fungal growth was evaluated by comparison of the dry cell weight with the normal growth in the control culture medium. The microbe suspension, 1 mL, was inoculated under aseptic conditions in 100 mL of liquid Sabouraud medium (1% peptone, 4% glucose) containing chitosan or its schiff's base that had been sterilized at 121 °C for 20 min. The control contained only liquid Sabouraud medium without chitosan. All the samples were incubated at 28 °C with shaking. The cultures were filtered every 12 h and the pellet was washed with distilled water and dried at 80 °C overnight. The dry cell weight was then determined. In the determination of the inhibition activity of chitosan and its schiff's base on growth of both *A. niger* and *Candida*

*albicans*, the microbe suspension, 1 mL, was inoculated into 100 mL of liquid Sabouraud medium containing chitosan with different concentrations. A blank without chitosan was prepared also for comparison. All the samples were incubated at 28 °C for 48 h. The cultures were filtered, and the pellet was washed with distilled water and dried at 80 °C to constant weight.

### 3. RESULTS AND DISCUSSION

#### 3.1. Characterization of the prepared hydrogels

The IR spectrum of the schiff's base - Fig. 1 - presented a strong absorption band at  $1632\text{ cm}^{-1}$  attributed to the  $-\text{CH}=\text{N}-$  vibrations characteristic of imines which is not observed in chitosan. The broad peak at  $3450\text{ cm}^{-1}$  corresponds to the stretching vibration of  $-\text{NH}$  and  $-\text{OH}$  bonds shifted to higher frequency and changed from doublet band of  $-\text{NH}_2$  to a single band for  $-\text{NH}$ . The characteristic absorption peak for  $-\text{NH}_2$  group at  $1600\text{ cm}^{-1}$  decreased in its intensity due to the decrease in its content indicating that the reaction on amino groups in chitosan with crotonaldehyde to give schiff's base.

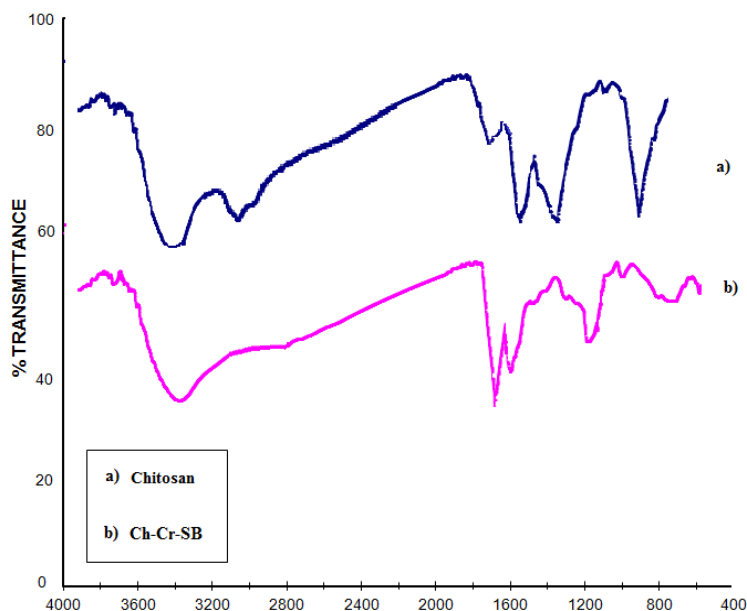


**Figure 1.** FTIR Chart of both Chitosan and Chitosan-Crotonaldehyde Schiff Base (Ch-Cr-SB).

TGA analyses - Fig. 2- showed that the initial decomposition temperature (*IDT*) of Chitosan (280 °C) is higher than Ch-Cr-SB (240 °C) and also the thermal degradation rate of Chitosan is much more better than its schiff's base with Crotonaldehyde; at Temperature 400 °C, the weight loss for Chitosan is about 43 % while the weight loss reaches almost 55 % for Ch-Cr-SB. This indicates that schiff's base polymers are less stable than Chitosan itself. It seems that the instabilities of schiff's base

polymers compared to chitosan are due to the absence of the free amino groups in the schiff's base polymers as they are replaced by  $-N=CH-$  groups.

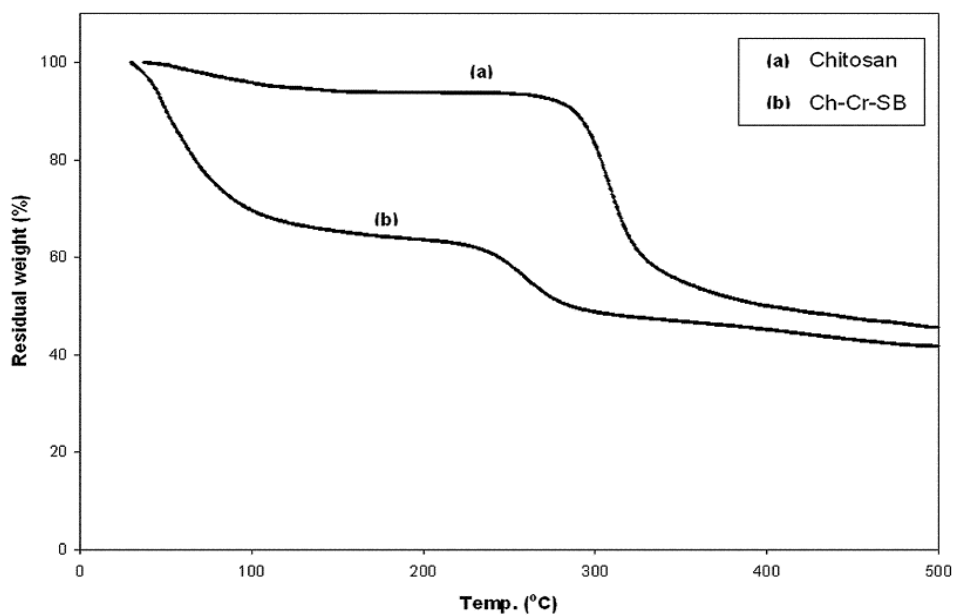


**Figure 2.** Thermogravimetric Analysis Curves of a) Chitosan and b) Chitosan-Crotonaldehyde Schiff base (Ch-Cr-SB).

Fig. 3 shows the X-ray diffraction patterns of chitosan and its schiff's base. The pattern of chitosan showed a strong characteristic sharp peak at  $2\theta = 20^\circ$ . For the schiff's base, that peak  $2\theta = 20^\circ$  gets much wider and weaker than in case of chitosan.

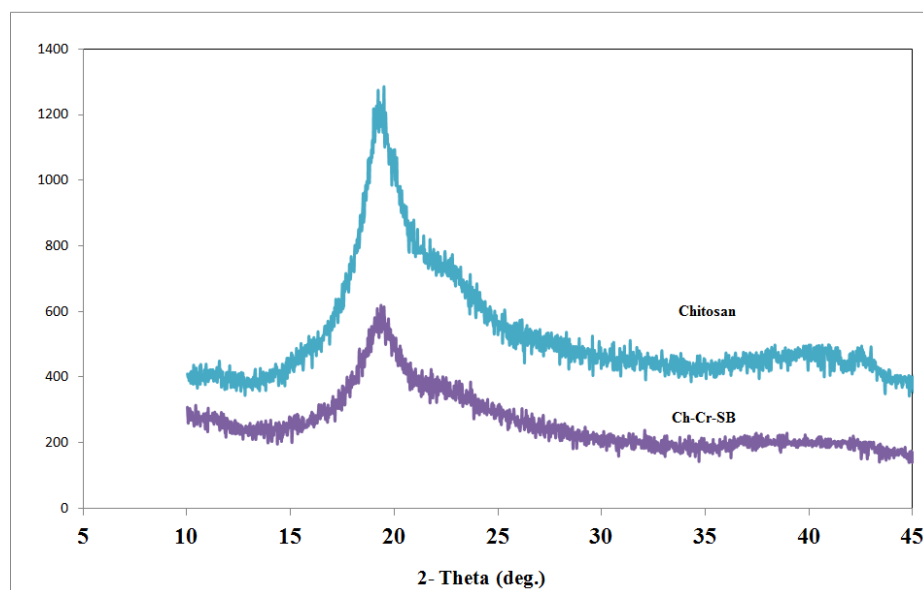


**Figure 3.** X-Ray Diffraction patterns of a) Chitosan and b) Chitosan-Crotonaldehyde Schiff base (Ch-Cr-SB).

This result indicates that the schiff's base is of poor crystallinity compared to the parent chitosan, which is attributed to the deformation of the strong hydrogen bonds in the chitosan backbone with the substitution of crotonaldehyde groups on the  $\text{NH}_2$  groups of chitosan.

### 3.2. Scanning electron microscopy

The scanning electron micrographs of both Chitosan and its schiff's base (Ch-Cr-SB) are shown in Fig 4 with magnification of (1000x). The flaky nature of chitosan was totally modified via the formation of schiff's base as the smooth surface was converted into porous-like surface for the prepared schiff base.

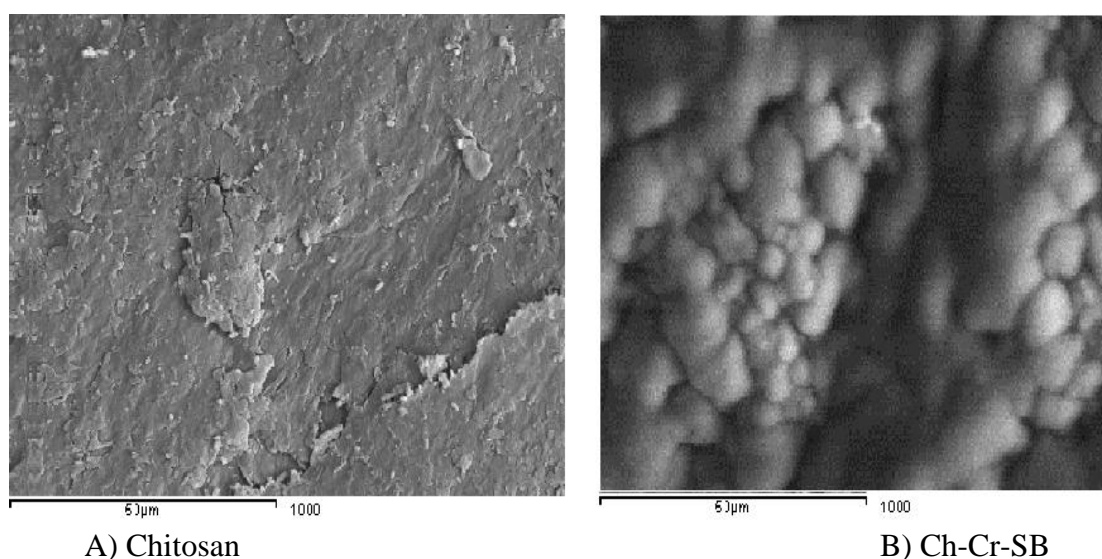


**Figure 4.** Scanning electron microscopy of a) Chitosan and b) Chitosan-Crotonaldehyde Schiff base (Ch-Cr-SB).

### 3.3. Applications done on the prepared hydrogels

#### 3.3.1. Water uptake

Chitosan swells much more in acidic medium (pH 4) than in basic medium (pH 9) due to the presence of the basic  $-\text{NH}_2$  groups in chitosan chains, its swellability in neutral pH is intermediate- as shown in Table 1-.

As for the Ch-Cr-SB hydrogel, its swellability in acidic medium is less than Chitosan itself due to the conversion of the basic amino groups in chitosan into  $-\text{N}=\text{CH}-$  groups, while Ch-Cr-SB swellability is more pronounced than that of chitosan in other pH values due to its hydrogel nature and due to the ability of forming more H-bondings with the surrounding media. This ability of hydrogels to swell in water, retaining a significant fraction of water within their structure without dissolving can

enable Ch-Cr-SB to be used as hydrogels in agricultural applications and various applications in the fields of medicine, pharmacy, biotechnology, and the controlled release of drugs.

**Table 1.** Water uptake by both Chitosan, Ch-Cr-SB in buffered solutions of different pH values.

Water uptake (%)					
Chitosan			Ch-Cr-SB		
pH 4	pH 7	pH 9	pH 4	pH 7	pH 9
700	450	140	580	600	519

### 3.3.2. Metal uptake

It was shown –Table 2- that the adsorption capacity for metal ions by Ch-Cr-SB is much greater than that of unmodified chitosan, due to the chemical modification of the  $-NH_2$  group of chitosan and its conversion into the more chelating  $-N=CH$  group, containing much more electronegative heteroatoms which can act as good chelating centres for more metal ions. Ch-Cr-SB polymer may be considered as a good candidate to develop as efficient biopolymer-based chelating adsorbents for water treatment or the recovery of metal ions from seawater.

**Table 2.** Metal ions uptake (%) for Chitosan and Chitosan-Crotonaldehyde Schiff's base.

Metal ions uptake (%)		
Metal ion	Chitosan	Ch-CrSB
Ni <sup>2+</sup>	90	100
Co <sup>2+</sup>	80	110
Cd <sup>2+</sup>	89	105
Cu <sup>2+</sup>	85	100

### 3.3.3. Dye uptake

As shown in both Figs. 5 and 6, the adsorption of unmodified Chitosan for Congo red dye (Acidic dye) is much better than its adsorption for Maxilon blue (Cationic dye) due to the presence of the basic amino group into its chains.

Whereas, the adsorption of both Maxilon blue (Cationic dye) and Congo red dye (Acidic dye) was much improved by the chemical modification of chitosan into Ch-Cr-SB due to the changing of the amino groups of the chitosan chains to  $-N=CH-$  group, giving the chance for more chelating centers to be created on the polymer chains which can attract much more dyestuff molecules. These chitosan-based biomaterials can be used for dye removal and these versatile biosorbents become

efficient adsorbents for dye removal as they have a high affinity for many classes of dyes including acidic and cationic dyes.

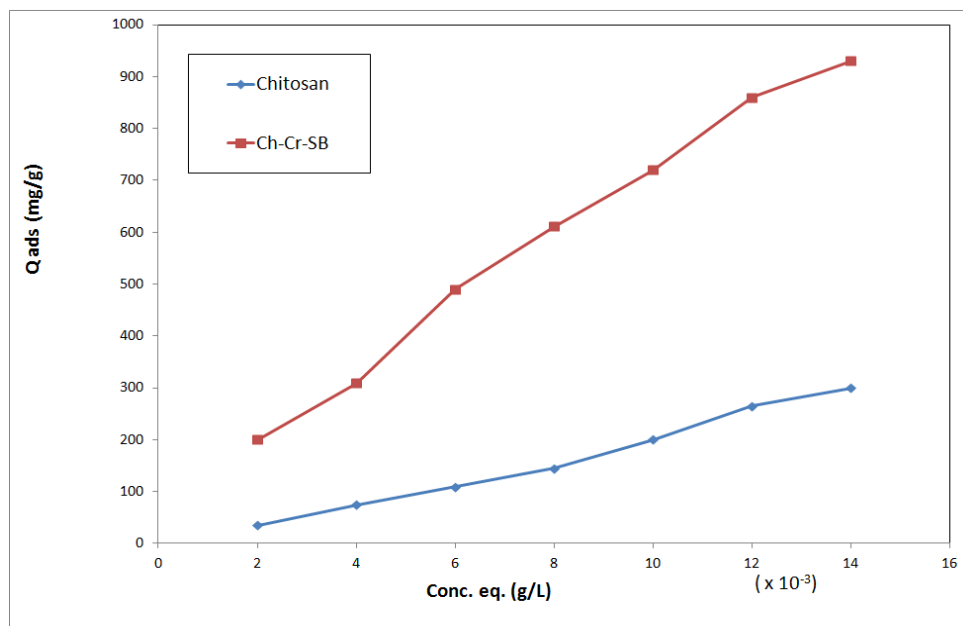


**Figure 5.** Variation of the amount of Maxilon Blue Dye adsorbed by Chitosan and Chitosan-Crotonaldehyde Schiff base (Ch-Cr-SB).

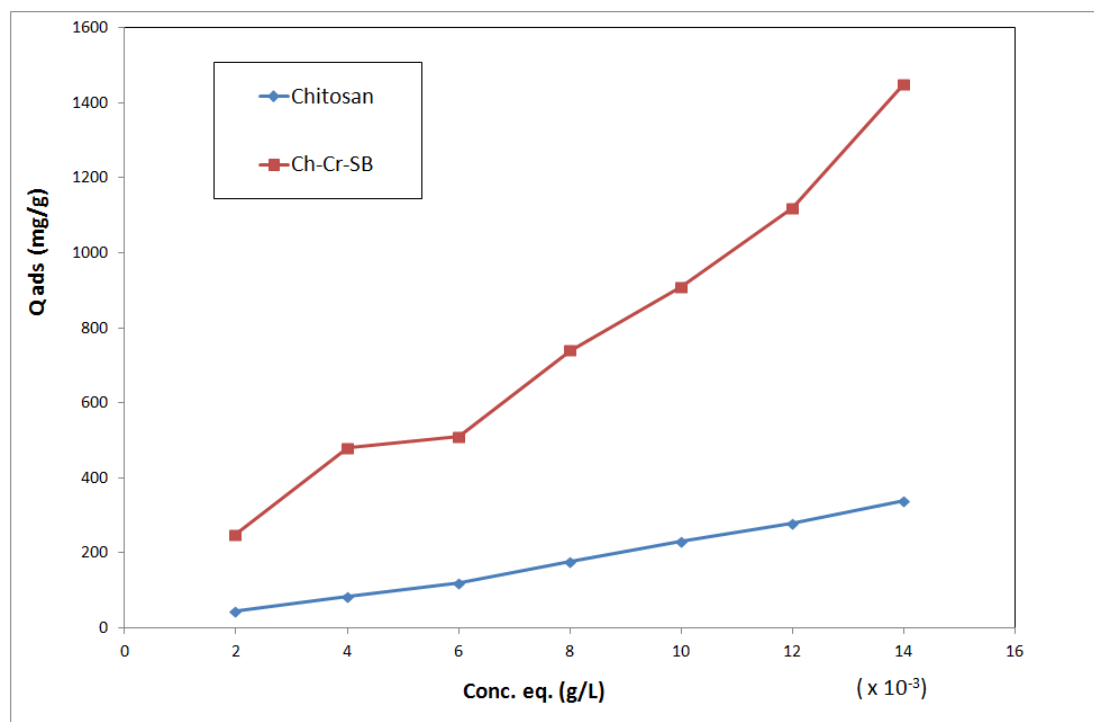


**Figure 6.** Variation of the amount of Congo Red dye adsorbed by Chitosan and Chitosan-Crotonaldehyde Schiff base (Ch-Cr-SB).

3.3.4. Antibacterial and antifungal activity

Both antibacterial and antifungal activity of chitosan and its schiff's base are shown in Table 3. The data indicated that both chitosan and its schiff's base have a good inhibiting effect on both *E. coli* and *S. aureus* but it was also found that the antibacterial activity of the schiff's base is stronger than that of chitosan itself. Also, The effect of chitosan and its schiff's base in inhibiting the growth of the *A. niger* and *Candida albicans* are listed in Table 3. There is no inhibiting effect at all observed for the native chitosan against the *A. niger*, while its schiff's base sample showed a good antifungal activity. It was also shown that the antifungal activity of the schiff's base against *Candida albicans* was stronger than that of chitosan.

**Table 3.** Antimicrobial activity for both Chitosan and its schiff base

Sample		Inhibition zone diameter (mm sample <sup>-1</sup> )			
		Esherichia coli (G <sup>-</sup> )	Staphylococcus aureus (G <sup>+</sup> )	A.niger (fungus)	Candida albicans (fungus)
Tetracycline	Standard	32	27	--	--
Antibacterial agent					
Amphotericin B		--	--	20	18
Antifungal agent					
Chitosan		21	19	-	9
Ch-Cr-SB		27	25	15	13

Antibacterial and antifungal activity of Ch-Cr-SB is found to be higher than that for Chitosan. Thus, a study of corrosion behavior of magnesium alloy (AZ91E) coated with Ch-Cr-SB has been done in artificial sea water. This is because Ch-Cr-SB coating isn't affected well by bacteria or fungi found on the medium as Chitosan coating. So, it can be used as inhibitor to protect magnesium alloy against corrosion in artificial sea water.

**4. CORROSION BEHAVIOR OF THE PREPARED SCHIFF BASE COATED AZ91E ALLOY**

4.1. Electrochemical impedance

4.1.1. Effect of concentration

The EIS scans measured after 2.5 h immersion in artificial sea water are displayed as Bode plots, in Fig. 7a and as Nyquist plots in Fig. 7b for AZ91E alloy depending on polymer concentration from 0.03 to 0.075 mM. Fig. 8a shows that the impedance ( $|Z|$ ) as well as the phase shift ( $\theta$ ) were found to increase by increasing (Ch-Cr-SB) polymer concentration. The results in general show that Bode plots display two maximum phase lag, at higher and lower frequencies regions, separated by an

inductive loop at intermediate frequencies. Inductive loops can be explained by the occurrence of adsorbed intermediate on the surface through heteroatoms as nitrogen or oxygen and  $\pi$  electrons on the double bonds and the alloy surface. In literature, it is well known that the effect of corrosion inhibition is related to the number of double bonds where inhibition efficiency increases when the inhibitor concentration or double bond number increases.

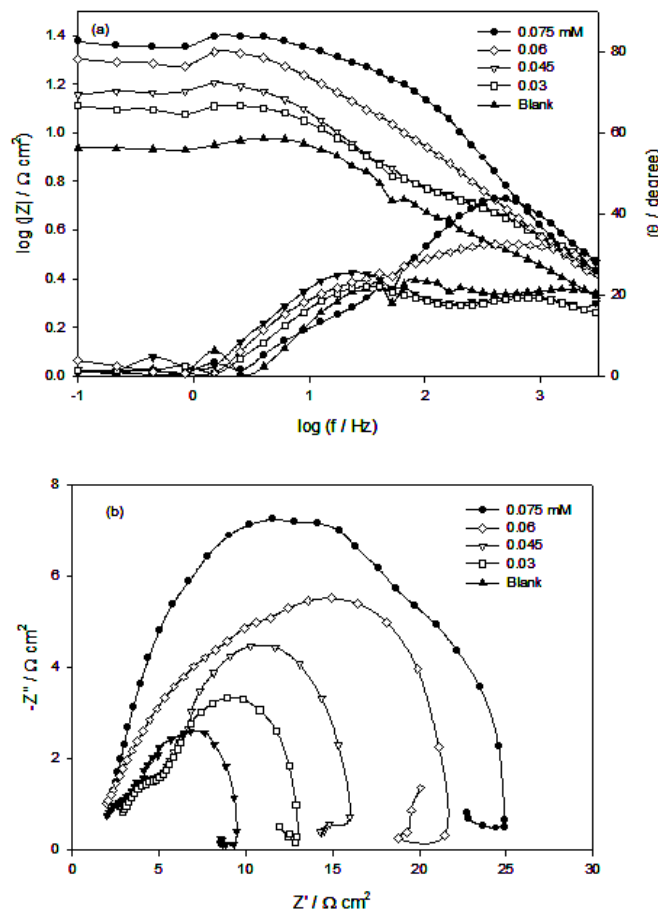
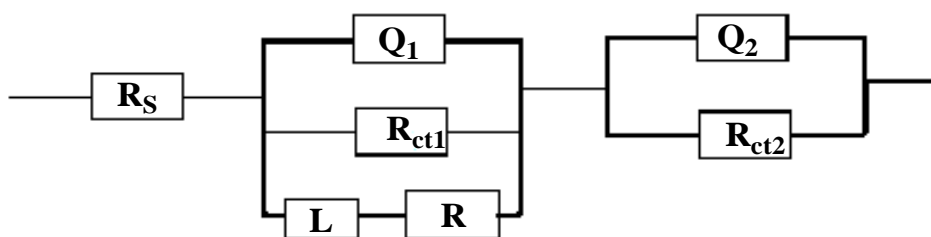


**Figure 7.** (a) Bode and (b) Nyquist plots of (Ch-Cr-SB)-coated AZ91E alloy with different polymer concentrations in artificial sea water.

High electron density of the double bonds in organic compounds helps the organic molecules to get chemisorbed on to the metal surface, thus the corrosion rate decreases [28]. This is also due to antimicrobial activity increases with increasing polymer concentration. The experimental data was consistent with the involvement of  $\text{Mg}^+$  as intermediate species in the magnesium dissolution at film imperfections. At such sites, magnesium first oxidised electrochemically to the intermediate species  $\text{Mg}^+$ , and then the intermediate species chemically reacted with water to produce hydrogen and  $\text{Mg}^{2+}$ . The first capacitive semicircle at higher frequencies is attributed to the redox  $\text{Mg}-\text{Mg}^+$  reaction since it was assumed to be the rate determining step in the charge transfer process, so it corresponds to the charge transfer resistance. On the other hand, the second capacitive semicircle could be attributed to the fast complementary corrosion reaction of  $\text{Mg}^+-\text{Mg}^{2+}$  and adsorption of active sites in polymer

molecule as  $-\text{NH}_2$ ,  $-\text{CH}_3$  and  $-\text{OH}$  groups on alloy surface with  $\text{Mg}^{2+}$ . Thus, increasing polymer concentration leads to an increase in the size of the capacitive semicircles, indicating an increase in the resistance value due to the increase in the adsorption strength through active groups as amino, hydroxyl, methyl group and electron pairs of double bonds. The increase in resistivity also arise from the change in chemical composition of the polymer surface film due to adsorption of active groups which protect alloy surface against bacteria, fungi and aggressive medium containing  $\text{Cl}^-$  ions.

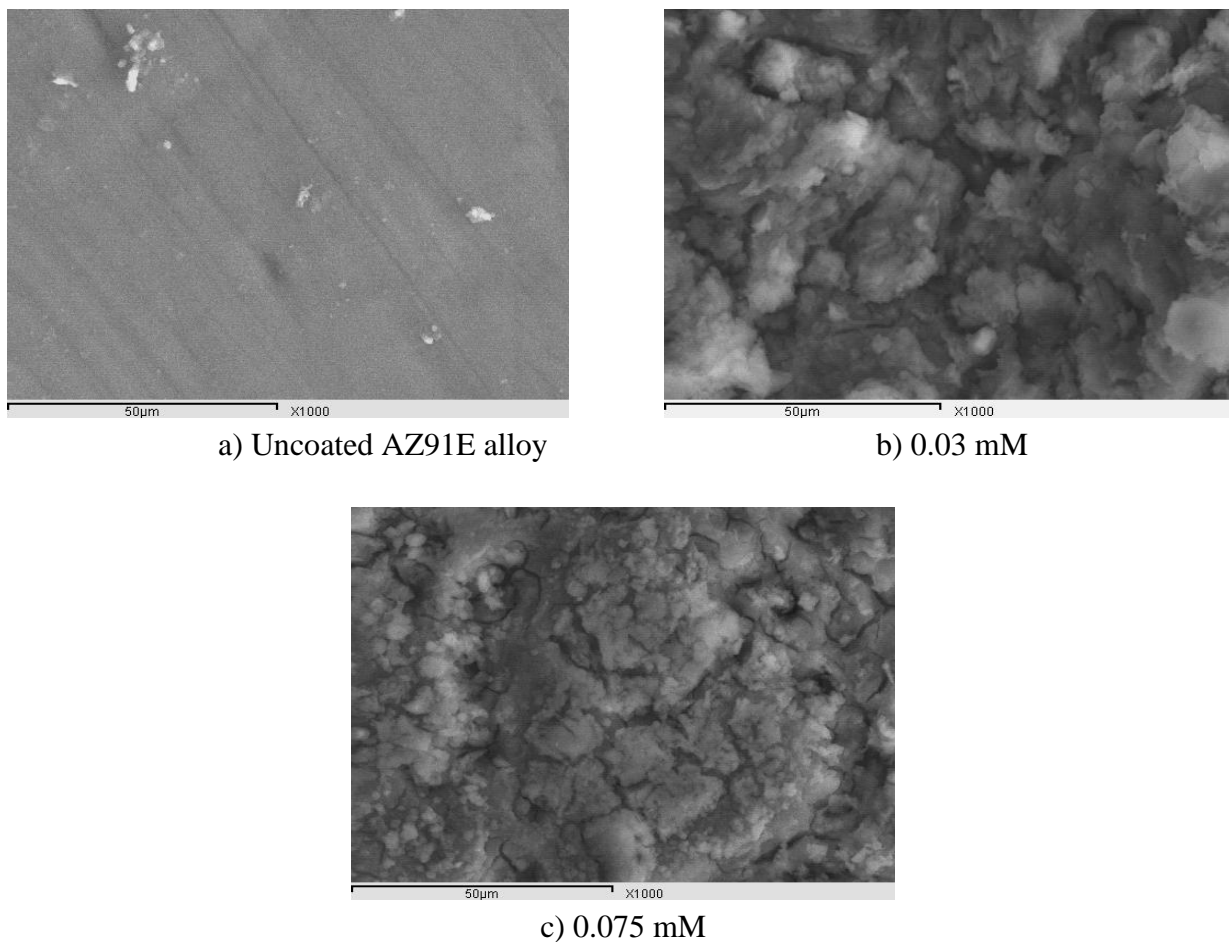
Also, it was found that the scavenging effect of schiff's base increases with the increase in its concentration [28] and this leads to an increase in corrosion resistance of the formed film. Also, its high antibacterial and antifungal activity means that the film doesn't affected by bacteria or fungi in the medium and this leads to a well decrease in corrosion rate of coated alloy than uncoated one. The impedance data were thus simulated to the appropriate equivalent circuit for the case with two time constants (Fig. 8).



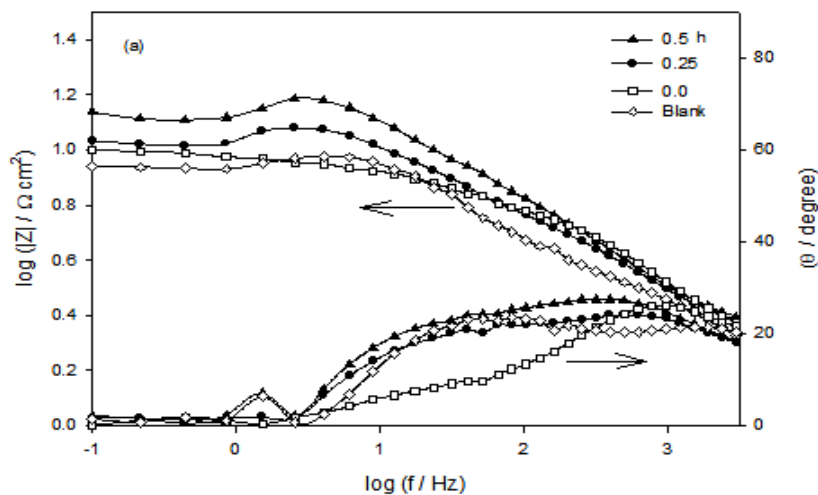
**Figure 8.** Equivalent circuit model representing two time constant for an electrode/electrolyte solution interface.

The model includes the solution resistance  $R_s$ , a series combination of resistance,  $R$ , and inductance,  $L$ , in parallel with charge transfer resistance  $(R_{ct})_1$ , and the constant phase element (CPE<sub>1</sub>). In the high frequency limit, the inductive contribution to the overall impedance is insignificant. Therefore, Nyquist plot (Fig. 7b) of the impedance is a semicircle characteristic of the parallel arrangement of the double layer capacitance and charge transfer resistance corresponding to the corrosion reaction. Contribution to the total impedance at intermediate frequencies comes mainly from the charge transfer resistance and inductive component in parallel. The inductor arise from adsorption effects could be defined as  $(L = R\tau)$  where  $\tau$  is the relaxation time for adsorption on electrode surface. The low frequency locus displays the characteristics of parallel RC circuit. This circuit includes another constant phase element (CPE<sub>2</sub>) which is placed in parallel to charge transfer resistance element  $(R_{ct})_2$ . The  $(R_{ct})_2$  value is a measure of charge transfer resistance corresponds to the  $\text{Mg}^+ - \text{Mg}^{2+}$  reaction and adsorption reaction. The CPE [29] is used in this model to compensate for non-homogeneity in the system and is defined by two values,  $Q$  and  $\alpha$ . The impedance of CPE is  $Z_{\text{CPE}} = Q^{-1}(i\omega)^{-\alpha}$ , where  $i = (-1)^{1/2}$ ,  $\omega$  is frequency in  $\text{rad s}^{-1}$ ,  $\omega = 2\pi f$  and  $f$  is the frequency in Hz,  $0 < \alpha < 1$ <sup>32</sup>. The fit results demonstrated in Table 7 with an average error of 3%. It was found that resistance values increase by increasing (Ch-Cr-SB) polymer concentration. This was confirmed by SEM

micrographs, Fig. 9a for uncoated alloy, Fig. 9b for 0.03 mM polymer concentration coated alloy and Fig. 9c for 0.075 mM concentration in artificial sea water.



**Figure 9.** SEM micrographs of (a) uncoated-AZ91E electrode; (b) (Ch-Cr-SB)-coated AZ91E with 0.03 mM polymer concentration and (c) 0.075 mM, after immersion for 2.5 h in artificial sea water at 298 K.



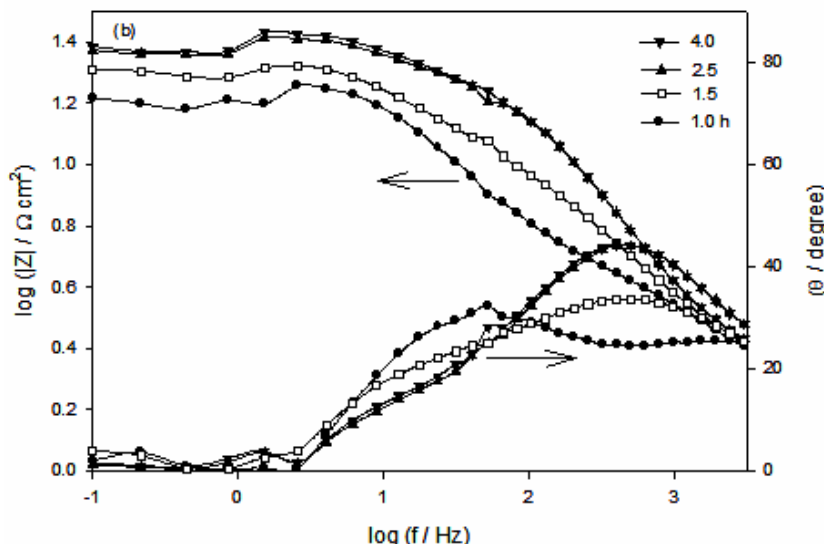


**Figure 10.** (a,b) Bode plots of 0.075 mM (Ch-Cr-SB)-coated AZ91E alloy with immersion time in artificial sea water

It was found that increasing polymer concentration leads to an increase in the film thickness formed on the alloy surface, thus, decreasing the corrosion rate of AZ91E alloy and this is clear from the micrograph for 0.03 mM concentration, where the film is porous but at 0.075 mM is nearly smooth and better.

The corrosion behavior of AZ91E alloy in artificial sea water containing 0.075 mM polymer concentration with immersion time of 4 hours is shown in Fig. 10a,b as Bode plots. The plots are fitted using the same equivalent circuit shown in Fig. 8. The value of  $|Z|$  and phase angle were found to increase with increasing immersion time suggesting that the formed surface film remains stable for 4 hours in aggressive chloride solution. This effect is more likely due to the coating absorbing water and swelling slightly, closing off pores that may be formed on the surface due to the aggressiveness of the medium or pores becoming clogged with corrosion product.

**Table 4.** Impedance and corrosion parameters of (Ch-Cr-SB)-coated AZ91E alloy in artificial sea water with different polymer concentrations, at 298 K.

C / mM	$R_s / \Omega\text{cm}^2$	$(R_{ct})_1 / \Omega\text{cm}^2$	$Q_1 / \mu\text{F cm}^{-2}$	$\alpha$	$R / \Omega\text{cm}^2$	L	$(R_{ct})_2 / \Omega\text{cm}^2$	$Q_2 / \mu\text{F cm}^{-2}$	$\alpha$	$i_{\text{corr}} / \mu\text{A/cm}^2$	$E_{\text{corr}} / \text{V}$
0.000	0.25	6.67	146.4	0.87	38.07	0.02	4.74	76.0	0.91	1384	-1.53
0.030	0.29	10.3	118.3	0.88	133.8	0.07	5.35	68.8	0.91	1161	-1.43
0.045	0.29	11.5	106.1	0.86	164.2	0.09	5.35	67.8	0.93	455.2	-1.32
0.060	0.30	18.6	52.04	0.87	255.1	0.14	5.61	39.8	0.92	308.3	-1.24
0.075	0.31	23.8	50.66	0.89	278.3	0.15	5.70	34.4	0.90	199.5	-1.17

4.1.2. Effect of temperature

EIS diagrams of AZ91E alloy in artificial sea water containing 0.075 mM (Ch-Cr-SB) concentration was investigated at different temperatures, displayed as Bode plots in Fig. 11 and fitted using equivalent circuit shown in Fig. 8. The data presented in Table 5, it can be seen that the resistance decreases with increasing the solution temperature due to dissolution occurs. This should be due to the replacement of (Ch-Cr-SB) polymer on the alloy surface by the aggressive chloride ions as contaminant by increasing the temperature and due to partial dissolution of the polymer from the metal surface [30]. The impedance measurements provide information on both the resistive and capacitive behavior of the interface and makes possible to evaluate the performance of (Ch-Cr-SB) coating as a protective layer against metal corrosion [31].

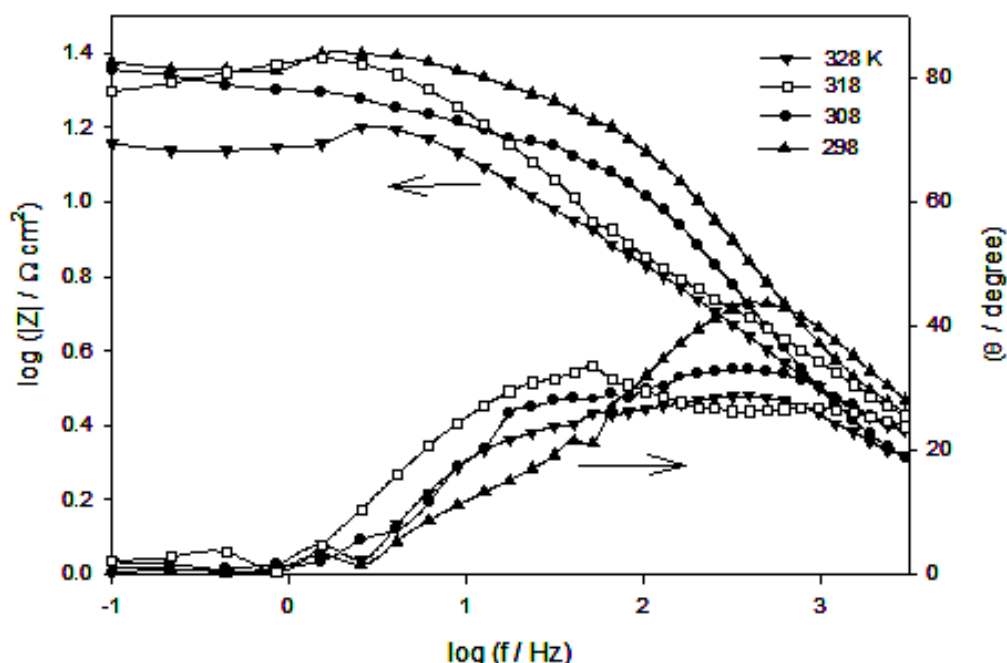


**Figure 11.** Bode plots of 0.075 mM (Ch-Cr-SB)-coated AZ91E alloy in artificial sea water at different temperatures.

**Table 5.** Impedance and corrosion parameters of 0.075 mM (Ch-Cr-SB)-coated AZ91E alloy in artificial sea water at different temperatures.

T / K	$R_s /$ $\Omega\text{cm}^2$	$(R_{ct})_1 /$ $\Omega\text{cm}^2$	$Q_1 /$ $\mu\text{F cm}^{-2}$	$\alpha$	R / $\Omega\text{cm}^2$	L	$(R_{ct})_2 /$ $\Omega\text{cm}^2$	$Q_2 /$ $\mu\text{F cm}^{-2}$	$\alpha$	$i_{\text{corr}}$ $\mu\text{A/cm}^2$	$E_{\text{corr}}$ V
298	0.31	23.8	50.66	0.89	278.3	0.15	5.70	34.4	0.90	199.5	-1.17
308	0.31	22.1	52.87	0.88	253.8	0.14	5.56	35.7	0.87	316.2	-1.28
318	0.30	19.2	53.23	0.87	247.2	0.12	4.18	38.4	0.89	1253	-1.32
328	0.31	15.5	59.45	0.88	227.3	0.11	2.15	45.9	0.89	1622	-1.36

## 4.2. Potentiodynamic polarization measurements

### 4.2.1. Effect of concentration

The electrochemical corrosion characteristics of AZ91E alloy in naturally aerated artificial sea water containing different concentrations of (Ch-Cr-SB) polymer at 298 K were investigated using a potentiodynamic technique as shown in Fig. 12 compared to the blank. For all tested concentrations, the active dissolution parameters including the values of the corrosion potential ( $E_{\text{corr}}$ ) and corrosion current density ( $i_{\text{corr}}$ ) are given in Table 4.

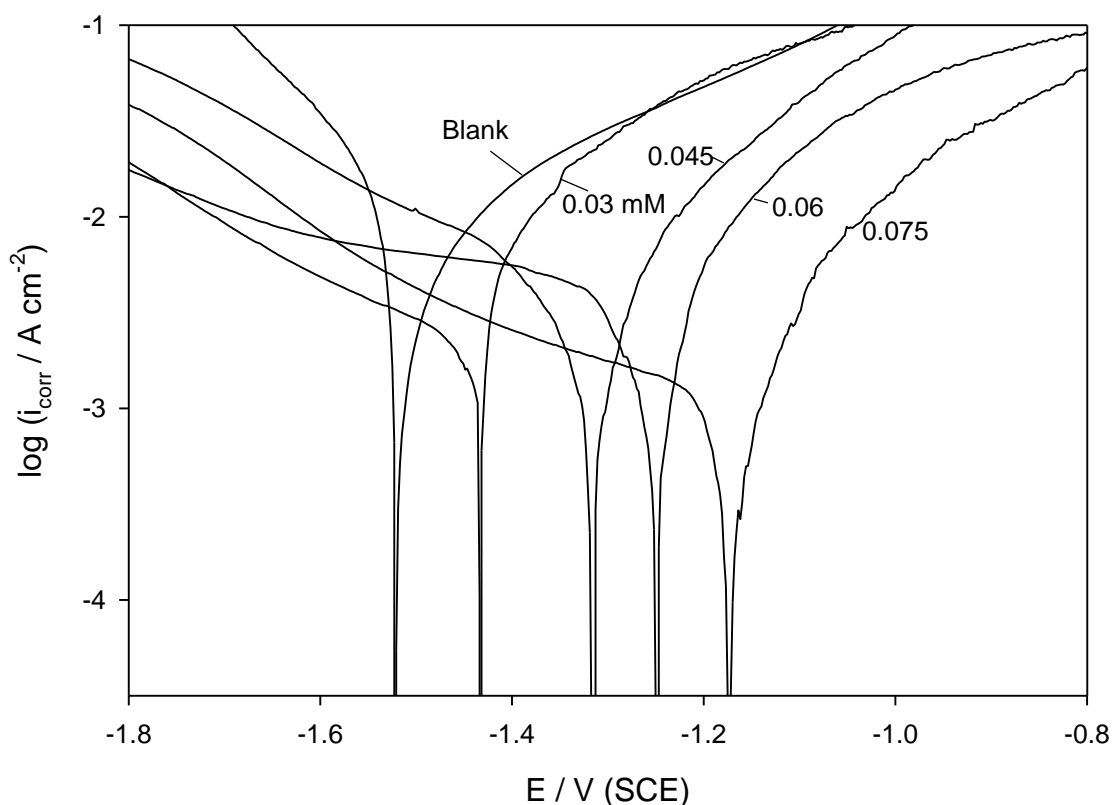


**Figure 12.** Potentiodynamic polarization scans of (Ch-Cr-SB)-coated AZ91E alloy with different polymer concentrations in artificial sea water.

The corrosion rate decreases than that for the blank due to polymer structure containing nitrogen and/or oxygen atoms can be strongly adsorbed on alloy surface [28]. Also, heterocyclic compounds containing nitrogen or oxygen atoms were found to be efficient inhibitors for corrosion in aggressive chloride media. The corrosion rate decreases with increasing polymer concentration due to adsorption of organic molecules on the metal surface increase, which takes place through the formation of bonds between the nitrogen electron pair and  $\pi$ -electrons and the metal surface, thereby reducing corrosion [28].

#### 4.2.2. Effect of temperature

To evaluate the adsorption of polymer and activation parameters of the corrosion processes of AZ91E in artificial sea water containing 0.075 mM Ch-Cr-SB, polarization parameters are investigated at temperature range of 298 to 328 K and presented in Table 5. Fig. 13 shows the polarization curve of 0.075 mM Ch-Cr-SB-coated AZ91E alloy at different temperatures.

The values of  $i_{\text{corr}}$  increase with temperature indicating activation in the dissolution process of the surface oxide film associated with a reduction in its protective properties.

This behavior may be attributed to some intrinsic modifications made by the film in its chemical composition and/ or physical structure [32]. Also, this behavior may be due to decreasing the adsorption of polymer active sites leading to an increase in the corrosion rate by the aggressive chloride ions present in the medium.

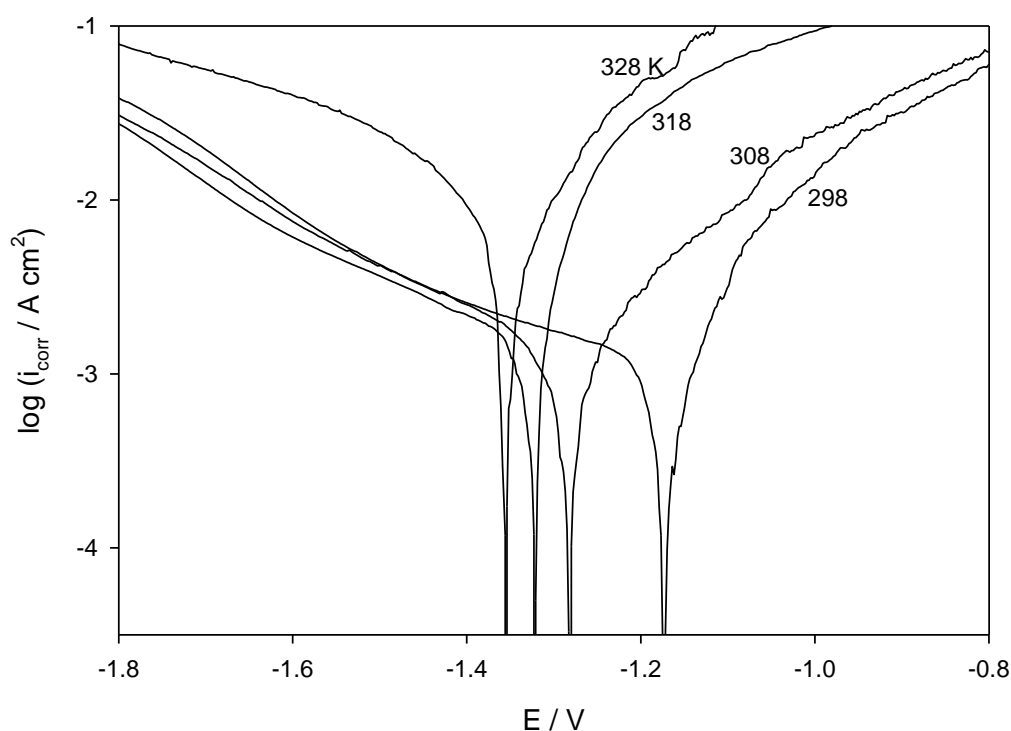


**Figure 13.** Potentiodynamic polarization scans of 0.075 mM (Ch-Cr-SB)-coated AZ91E alloy in artificial sea water at different temperatures.

## 5. CONCLUSIONS

A novel schiff's base of chitosan (Ch-Cr-SB) was synthesized via reaction of chitosan with crotonaldehyde. Characterization of the produced polymer was done by different analyses. The water uptake results indicated the high swellability for Ch-Cr-SB polymer compared to parent Chitosan in neutral and basic pH values, which enables it to be used in various applications. Ch-Cr-SB was

investigated as a better adsorbent than unmodified chitosan for various metal ions like; Ni<sup>2+</sup>, Co<sup>2+</sup>, Cd<sup>2+</sup> and Cu<sup>2+</sup>. Also Ch-Cr-SB was investigated as a better adsorbent than native chitosan for various dyestuffs like; *Congo red dye* and *Maxilon Blue dye*. The antimicrobial activity results of chitosan and its schiff's base against *E. coli*, *S. aureus*, *A. niger* and *Candida albicans* indicated that Ch-Cr-SB has better antimicrobial activities than native chitosan.

Corrosion rate for AZ91E in artificial sea water increased with increasing the polymer concentration or increasing time of immersion. Also, Corrosion rate for AZ91E in 3% NaCl increased with decreasing temperature for 0.075 mM polymer concentration. This allows Ch-Cr-SB polymer to be used as a coating to AZ91E alloy for different applications in sea water (3 % NaCl).

## References

1. S. Hirano, K. Nagamura, M. Zhang, S.K. Kim, B.G. Chung and M. Yoshikawa, *Carbohydr. Polym.* 8 (1999) 293.
2. K. Kurita, S. Mori, Y. Nishiyama and M. Harata, *Polym. Bull.* 48 (2002) 159.
3. G. K. Moore and G.A.F. Roberts, *Intern. J. of Bio. Macromol.* 3 (1981) 337.
4. H. Sashiwa and Y. Shigemasa, *Carbohydr. Polym.*, 39 (1999)127.
5. Z.Cimerman and N. Galic, B. Bosner, *Anal. Chim. Acta*, 343 (1997) 145.
6. Y. Baba, Y. Kawano and H. Hirakawa, *Bull. of Chem. Soc. of Japan*, 69 (1996) 1255.
7. Z.Yang and Y.Yuan, *J. of Appl. Poly. Sci.*, 82 ( 2001) 1838.
8. T. Becker, M. Schlaak and H. Strasdeit, *Reactive & Functional Polym.*, 44 (2000) 289.
9. L.D. Hall and M. Yalpani, *Carbohydrate Research*, 83 (1980) C<sub>5</sub>.
10. D.D. Hu, Q.Z. Shi, Y. Tang Fang and J.F. Kennedy, *Carbohydr. Polym.*, 45 (2001) 385.
11. C.A.Rodrigues, M.C.M. Laranjeira, V.T.De Favere, E.Stadler, *Polymer*,39 (1998) 5121.
12. J.E.Santos, E.R.Dockal and E.T.G.Cavalheiro, *J. of Thermal Anal. and Calorimetry* 79 (2005) 243.
13. A.A. Soliman, *J. of Thermal Analy. and Calorimetry*, 63 (2001) 221.
14. F.A.A. Tirkistani, *Polym. Degradn. and Stability*, 61 (1998) 161.
15. L.S. Guinesi, É.T.G. Cavalheiro, *Carbohydrate Polym.*,65 (2006) 557.
16. G.Crini, *Bioresource Technology*, 97 (2006) 1061.
17. G.Crini, *Prog. in Polym. Sci.*, 30 (2005) 38.
18. M. Prabakaran and J. F. Mano, *Carbohydrate Polym.*, 63 (2006) 153.
19. I.Uzun and F. Güzel, *J. of Colloid Intern. Sci.* 274 (2004) 398.
20. M.S. Chiou and G.S. Chuang, *Chemosphere* 62 (2006) 731.
21. C. Chang and D. H. Chen, *Macromolecular Biosciences* 5 (2005) 254.
22. Y.Shimizu, S.Tanigawa, Y. Saito and T. Nakamura, *J. of Appl. Polym. Sci.* 96 (2005) 2423.
23. A.D.Südholz, N.Birbilis, C.J. Bettles and M.A. Gibson, *J. of Alloys and Cpds.*, 471 (2009) 109.
24. M.A. Fekry and M.Z. Fatayerji, *Electrochim. Acta.* 54 (2009) 6522.
25. M.A. Fekry and R.M. El-Sherief, *Electrochem. Acta* 54 (2009) 7280.
26. M. A. Fekry, *Intern. J. of Hyd. Ener.* 35 (2010) 12945.
27. J. E. dos Santos , E. R. Dockal and E.T.G. Cavalheiro, *Carbohydr. polym.* 60 (2005) 277.
28. E.E.Ebenso, U.J.Ekpe, B.I.Ita, O.E. Offiong and U.J. Ibok, *Maters. Chem. Phys.*, 60 (1999) 79.
29. M.A. Fekry, *Electrochim. Acta* 54 (2009) 3480.
30. Z.Guo, R.Xing, S.Liu, H. Yu, P. Wang, C. Li and P. Li , *Bioorg. & Med. Chem. Letters* 15 (2005) 4600.
31. K.C. Emregül and M. Hayvalı, *Corros. Sci.* 48 (2006) 797.

32. S.L.A. Maranhao, I.C. Guedes, F.J. Anaissi, H.E.Toma and I.V. Aoki, *Electrochim. Acta*, 52 (2006) 519.